Naval Research Laboratory

Washington, DC 20375-5320

NRL/MR/6790--09-9187

Wall-Plug Efficiencies of High-Power Free Electron Lasers Employing Energy Recovery Linacs

PHILLIP SPRANGLE
JOSEPH PEÑANO

Beam Physics Branch
Plasma Physics Division

BAHMAN HAFIZI

Icarus Research, Inc.
Bethesda, Maryland

ILAN BEN-ZVI

Brookhaven National Laboratory
Upton, New York

April 23, 2009

REPORT DOCUMENTATION PAGE

Form Approved
OMB No 0704-0188

1 REPORT DATE *(DD-MM-YYYY)*	2 REPORT TYPE	3 DATES COVERED *(From - To)*
23-04-2009	Interim	April 2008 – April 2009

4 TITLE AND SUBTITLE

Wall-Plug Efficiencies of High-Power Free Electron Lasers Employing Energy Recovery Linacs

5a CONTRACT NUMBER

5b GRANT NUMBER

5c PROGRAM ELEMENT NUMBER

6 AUTHOR(S)

Phillip Sprangle, Joseph Peñano, Bahman Hafizi,* and Ilan Ben-Zvi†

5d PROJECT NUMBER
67-9252-09

5e TASK NUMBER

5f WORK UNIT NUMBER

7 PERFORMING ORGANIZATION NAME(S) AND ADDRESS(ES)

Naval Research Laboratory, Code 6790
4555 Overlook Avenue, SW
Washington, DC 20375

8 PERFORMING ORGANIZATION REPORT NUMBER

NRL/MR/6790--09-9187

9 SPONSORING / MONITORING AGENCY NAME(S) AND ADDRESS(ES)

Office of Naval Research
One Liberty Center
875 North Randolph Street
Arlington, VA 22203-1995

10 SPONSOR / MONITOR'S ACRONYM(S)

ONR

11 SPONSOR / MONITOR'S REPORT NUMBER(S)

12 DISTRIBUTION / AVAILABILITY STATEMENT

Approved for public release, distribution is unlimited

13 SUPPLEMENTARY NOTES

*Icarus Research, Inc , P O Box 30780, Bethesda, MD 20824
†Brookhaven National Laboratory, Upton, NY 11973-5000

14 ABSTRACT

In a high average power free electron laser (FEL) the wall-plug efficiency is of critical importance in determining the size, complexity and cost of the overall system The wall-plug efficiency for the FEL oscillator and amplifier (uniform and tapered wiggler) are strongly dependent on the energy recovery process A theoretical model for electron beam dynamics in the energy recovery linac is derived and applied to the acceleration and de-acceleration of nano-Coulomb electron bunches for a tapered FEL amplifier For the tapered amplifier, the spent electron beam exiting the wiggler consists of trapped and untrapped electrons De-accelerating these two populations using different phases of the radio-frequency wave in the recovery process enhances wall-plug efficiency For the parameters considered here, the wall-plug efficiency for the tapered amplifier can be -40% using this method

15 SUBJECT TERMS

Free-electron laser
Tapered amplifier
Wall-plug efficiency
Energy recovery linac

16 SECURITY CLASSIFICATION OF:			17 LIMITATION OF ABSTRACT	18 NUMBER OF PAGES	19a NAME OF RESPONSIBLE PERSON
a REPORT	b ABSTRACT	c THIS PAGE			Phillip Sprangle
Unclassified	Unclassified	Unclassified	UL	26	19b TELEPHONE NUMBER *(include area code)* (202) 767-3493

Standard Form 298 (Rev 8-98)
Prescribed by ANSI Std Z39 18

THIS PAGE INTENTIONALLY LEFT BLANK

TABLE OF CONTENTS

Wall-Plug Efficiencies of High-Power Free Electron Lasers Employing Energy Recovery Linacs

Phillip Sprangle, Joseph Peñano, Bahman Hafizi[1] and Ilan Ben-Zvi[2]

Plasma Physics Division
Naval Research Laboratory
Washington DC

Abstract

In a high average power free electron laser (FEL) the wall-plug efficiency is of critical importance in determining the size, complexity and cost of the overall system. The wall-plug efficiency for the FEL oscillator and amplifier (uniform and tapered wiggler) are strongly dependent on the energy recovery process. A theoretical model for electron beam dynamics in the energy recovery linac is derived and applied to the acceleration and de-acceleration of nano-Coulomb electron bunches for a tapered FEL amplifier. For the tapered amplifier, the spent electron beam exiting the wiggler consists of trapped and untrapped electrons. De-accelerating these two populations using different phases of the radio-frequency wave in the recovery process enhances wall-plug efficiency. For the parameters considered here, the wall-plug efficiency for the tapered amplifier can be ~ 40% using this method.

1. *Icarus Research, Inc., Bethesda, MD*
2. *Brookhaven National Laboratory, Upton, NY*

I. Introduction

The purpose of this paper is to obtain estimates of the wall-plug efficiencies for high-power free electron lasers (FELs) employing energy recovery linacs (ERL). The FEL wall-plug efficiency can be substantially increased by use of ERLs [1]. For high-power FELs, the wall-plug efficiency is of major importance in determining the overall size and cost of the system. The power flow diagram for an FEL based on an ERL is shown schematically in Fig. 1. In Fig.1 the injected electron beam is accelerated by radio-frequency (RF) fields in the ERL and sent to the FEL interaction region. The spent electron beam from the FEL is sent back to the RF section and decelerated, thereby replenishing the RF field. The decelerated beam is then sent to a beam dump. In what follows, we define the wall-plug efficiency and calculate it for the FEL oscillator and amplifier (uniform and tapered wiggler) configurations.

II. Wall-Plug Efficiency

In the steady state, the following power balance relationship holds for the various powers flowing through the closed dashed curve in Fig.1,

$\eta(P_{WP} - P_{cryo}) = P_{FEL} + P_{dump}$, where $\eta = (1-\varepsilon)\eta_{\rm inj} + \varepsilon\eta_{\rm RF}$ is a combined efficiency, P_{WP} is the wall-plug power, P_{cyro} is the power for the cryogenics, magnets, etc., P_{FEL} is the FEL radiation power and P_{dump} is the electron beam power entering the dump. The combined efficiency η represents the efficiency of generating the RF fields for the injector and ERL as well as for generating the injected electron beam. Here η_{RF} is the efficiency of generating RF, ε is the fraction of power going into RF generation and η_{inj} is the efficiency of the injector (see Fig. 1). Note that the efficiency terms $(1-\varepsilon)\eta_{inj}$ and $\varepsilon\eta_{RF}$ are not independent of each other. The acceleration factor in ERL is given by $1+\varepsilon\eta_{RF}/(1-\varepsilon)\eta_{inj}$, which is assumed to be given. For example, if the initial electron beam is accelerated by a factor of 15, then the ratio $\varepsilon\eta_{RF}/(1-\varepsilon)\eta_{inj} = 14$. Using the above power balance relationship the wall-plug efficiency is given by

$$\eta_{\rm WP} = P_{\rm FEL}/P_{\rm WP} = G\eta_{\rm FEL}, \qquad (1a)$$

where the gain factor is

$$G = \frac{\eta}{\eta_{\rm FEL} + P_{\rm dump}/P_{\rm b} + \eta P_{\rm cryo}/P_{\rm b}}, \qquad (1b)$$

P_b is the electron beam power entering the FEL wiggler and $\eta_{\rm FEL} = P_{\rm FEL}/P_b$ is the FEL interaction efficiency. In obtaining the wall-plug efficiency, synchrotron radiation losses and halo formation, among other things, have been neglected. These effects can be easily included when estimating the system efficiencies. Typical values for the combined efficiency are $\eta \sim 0.4 - 0.6$ and $\eta P_{cryo}/P_b \sim 10^{-2}$. In this paper we take the average beam current to be I_b, the beam energy $E_b = 80\,\mathrm{MeV}$, $E_{\rm min} = 3\,\mathrm{MeV}$, and $P_{cryo} = 1\,\mathrm{MW}$ (for $I_b = 1\,\mathrm{A}$). In general, the wall-plug efficiency can be far higher than the FEL interaction efficiency, η_{FEL}, when an ERL is employed, i.e., $G > 1$. The wall-plug efficiency however is always less than η.

The beam power entering the beam dump, P_{dump}, depends on the FEL interaction, phase space manipulation of the electrons upon exiting the wiggler and the subsequence deceleration in the ERL. The deceleration in the ERL depends on the RF phase, self fields, longitudinal and transverse emittances as well as external focusing fields. These effects will be address in detail in Sections III and IV.

Within the FEL interaction region the electron beam loses energy and develops an energy spread. In addition to this induced energy spread the beam has an initial intrinsic energy spread which is typically < 1 % of the beam energy and is neglected. There is a minimum energy, $E_{\rm min}$, that the electrons can be decelerated to in the ERL. This minimum energy limit is due to various effects, such as, excessive electron de-phasing in the RF field and transverse emittance blowup.

a) Oscillator

Consider first an untapered FEL oscillator [2] and the associated wall-plug efficiency with an ERL [1, 3]. The optical energy is $P_{FEL} = \eta_{FEL} P_b$ where the optical efficiency in the low gain regime is $\eta_{FEL} = 1/(2N_w)$ and N_w is the number of wiggler periods. The electron beam energy exiting the decelerating RF fields within the ERL and entering the beam dump is $P_{dump} = I_b(E_{\rm min} + \delta E_{osc}/2)$, where δE_{osc} is the induced

electron beam energy spread. In an FEL oscillator the energy spread is proportional to the optical energy, αE_{FEL}, where $\alpha > 1$. The electron beam energy spread entering the ERL can be reduced by a factor β and is $\delta E_{osc} = \beta\alpha\eta_{FEL} E_b$. The phase space cooling parameter β accounts for the reduction in energy spread due to the spatial spreading of the beam outside of the wiggler. The wall-plug efficiency associated with the oscillator is

$$\eta_{WP} = G\eta_{FEL} = \frac{\eta\eta_{FEL}}{\eta_{FEL}(1+\alpha\beta/2) + P_{\min}/P_b + \eta P_{cryo}/P_b}. \qquad (2)$$

As an illustration, we take $N_w = 25$, $\alpha = 4$, $\beta = 1$, $E_b = 80$ MeV, $I_b = 1$ A, $P_{cryo} = 1$ MW, $\eta = 0.6$, and $E_{\min} = 2$ MeV and find that the FEL oscillator interaction efficiency is $\eta_{FEL} = 2\%$, and the wall-plug efficiency is $\eta_{WP} = 10\%$. Since the oscillator efficiency is $\sim 1/(2N_w)$, reducing N_w can increase the wall-plug efficiency. However, in the low gain regime the gain/pass is proportional to N_w^3 and therefore N_w cannot be reduced below the oscillator's start current condition.

b) Amplifier

The efficiency of an FEL amplifier can be high in the high-gain regime in which the radiation initially grows exponentially. The efficiency can be further increased by tapering the wiggler or by frequency detuning. In addition, pulse slippage is significantly reduced compared to the low gain oscillator regime [4]. Furthermore, in a high-gain uniform wiggler amplifier the radiation can be optically guided if the electron current is sufficiently high [4]. In a tapered wiggler amplifier, optical guiding can also be achieved even in the trapped particle regime.

i) Uniform Wiggler

The wall-plug efficiency associated with the untapered wiggler amplifier is

$$\eta_{WP} = \frac{\eta\eta_{FEL}}{\eta_{FEL}(1+\alpha\beta/2) + P_{\min}/P_b + \eta P_{cryo}/P_b} \qquad (3)$$

where the electron beam power entering dump is $P_{dump} = I_b(E_{\min} + \delta E_{amp}/2)$ and the induced energy spread is $\delta E_{amp} = \beta\alpha\eta_{FEL} E_b$. The FEL interaction efficiency, η_{FEL}, in a

uniform wiggler amplifier can be increased by approximately a factor of ~ 1.5 by frequency detuning [4].

ii) Tapered Wiggler

The wall-plug efficiency in the tapered wiggler amplifier configuration depends in detail on the bunch dynamics in the ERL. This analysis is presented in Section III. However, by making a number of simplifying assumptions an approximate expression for the wall-plug efficiency can be obtained. A more accurate values for the wall-plug is presented in Section IV.

In a tapered wiggler amplifier the FEL output power is [4, 5]

$$P_{FEL} = \eta_{FEL} P_b = \eta_{trap} \Delta P_b , \tag{4}$$

where $\eta_{FEL} = \eta_{trap} \Delta P_b / P_b$ is the FEL interaction efficiency, η_{trap} is the trapping efficiency, i.e., fraction of electrons trapped in the ponderomotive bucket, and $\Delta P_b = I_b \Delta E_b$ and ΔE_b is the change in the electron beam energy (tapered wiggler) associated with the trapped electrons. Figure 2 shows a sketch of the electron energy distribution in a tapered wiggler amplifier indicating the various stages of the trapped an untrapped electrons. If both the trapped and untrapped electrons are equally decelerated and the energy spreads are unchanged in the ERL, the electron beam energy entering the beam dump is $E_{dump} = \eta_{trap}(E_{\min} + \delta E_{trap}/2) + (1-\eta_{trap})(\Delta E_b + E_{\min} + \delta E_{trap}/2)$, which can be rewritten as

$$E_{dump} = (1 - \eta_{trap})\Delta E_b + E_{\min} + \delta E_{trap}/2 , \tag{5}$$

where δE_{trap} is the induced full energy spread associated with the trapped electrons. Note that to this level of approximation E_{dump} is independent of δE_{untrap}. The energy spread associated with the trapped electrons is

$$\delta E_{trap} \approx \beta \left(\frac{a_w}{1 + a_w^2/2} \right)^{1/2} a_R^{1/2} (E_b - \Delta E_b), \tag{6}$$

where $a_R = 6\times10^{-10}\, \lambda[\mu\text{m}] I_{peak}^{1/2}[\text{W/cm}^2]$ is the normalized vector potential associated with the optical field of wavelength λ, and a_w is the wiggler strength parameter. For a high average power FEL, the peak optical intensity within the wiggler is

$I_{peak} = 2P_{peak}/(\pi R_L^2) \approx 10^{10}$ W/cm^2 ($a_R \sim 10^{-4}$) where R_L is the laser spot size, and the fractional trapped electron energy spread is $\delta E_{trap}/E_b \approx 10^{-2}$.

The wall-plug efficiency associated with the tapered wiggler FEL amplifier becomes

$$\eta_{WP} = \frac{\eta\eta_{FEL}}{\eta_{FEL}/\eta_{trap} + P_{\min}/P_b + \delta E_{trap}/2E_b + \eta P_{cryo}/P_b}, \tag{7}$$

where we used the relation in Eq.(4).

III. Dynamics of a Charge Bunch in an ERL

The longitudinal and transverse dynamics of a relativistic charge bunch are described by a set of coupled envelope equations for the root mean square (rms) bunch length and radius. The bunch length and radius dynamics are determined by the effects of the RF linac field, space charge fields, inductive (self magnetic) fields, external focusing fields as well as the axial and transverse energy spreads (emittances).

The space charge and RF fields acting on the electron bunch are given in the Appendix. The axial and radial self electric fields with respect to the center of the bunch are

$$E_{SC,z}(z,t) = \frac{3}{5\sqrt{5}}\frac{qN}{R_b^2 L_b}M(\xi)(z - z_c(t)), \tag{8a}$$

$$E_{SC,r}(r,t) = \frac{3}{10\sqrt{5}}\frac{qN}{R_b^2 L_b}(1 - M(\xi))r, \tag{8b}$$

where the function $M(\xi)$ depends on the bunch's aspect ratio, energy and surrounding geometry (see Fig. 3 and the Appendix), qN is the bunch charge, L_b and R_b are the rms bunch length and radius in the laboratory frame and $z_c(t)$ is the axial position of the bunch centroid. In the absence of walls $M(\xi)$ is a function of the aspect ratio and energy only,

$$M(\xi) = \frac{1-\xi^2}{2\xi^3}\left(\ln\left(\frac{1+\xi}{1-\xi}\right) - 2\xi\right), \tag{9}$$

where $\xi = (1 - R_b^2/(\gamma L_b)^2)^{1/2}$. The express for $M(\xi)$ in Eq.(9) is valid for the full range of $R_b/(\gamma L_b)$. However, for the parameters considered in this paper $R_b/(\gamma L_b) << 1$, $R_b \sim L_b$, and $M(\xi) \approx -\xi^2(0.31 + \ln\xi)$.

The ERL fields are given by

$$E_{RF,z}(z,t) = E_{RF}\sin(\Psi_c), \tag{10a}$$

$$E_{RF,r}(r,z,t) = -E_{RF}(k_{RF}\, r/2)\cos(\Psi_c), \tag{10b}$$

$$B_{RF,\theta}(r,z,t) = -E_{RF}(\omega_{RF}\, r/2c)\cos(\Psi_c), \tag{10c}$$

where E_{RF} is the field amplitude, $\Psi_c = \int_0^z (k_{RF}(z') - \omega_{RF}/c\beta_c(z'))dz' + \Psi_c(0)$ is the phase, ω_{RF} is the RF frequency and $k_{RF} = 2\pi/\lambda_{RF}$ is the local wavenumber of the RF field.

The envelope equations are derived in the Appendix and are given by

$$\frac{\partial^2 L_b}{\partial z^2} + \left(3 + \frac{1}{\beta_c^2\gamma_c^2}\right)\frac{1}{\gamma_c}\frac{\partial\gamma_c}{\partial z}\frac{\partial L_b}{\partial z} - K_z^2 L_b - \frac{\varepsilon_{n,z}^2}{\beta_c^2\gamma_c^6 L_b^3} = 0, \tag{11a}$$

$$\frac{\partial^2 R_b}{\partial z^2} + \frac{1}{\beta_c^2\gamma_c}\frac{\partial\gamma_c}{\partial z}\frac{\partial R_b}{\partial z} - K_\perp^2 R_b - \frac{\varepsilon_{n,\perp}^2}{\beta_c^2\gamma_c^2 R_b^3} = 0, \tag{11b}$$

where $K_z^2 = K_{RF}^2\cos\Psi_c + K_{sc,z}^2$, $K_\perp^2 = K_{sc,\perp}^2 - K_Q^2 - K_{RF,\perp}^2$, $K_{sc,z}^2 = 3/(5\sqrt{5})q^2 N/(mc^2)M(\xi)/(\beta_c^2\gamma_c^3 R_b^2 L_b)$, $K_{RF}^2 = qE_{RF}\,k_{RF}/(mc^2\beta_c^2\gamma_c^3)$, $K_{sc,\perp}^2 = 3/(10\sqrt{5})q^2 N/(mc^2)(1 - M(\xi))/(\beta_c^2\gamma_c^3 R_b^2 L_b)$. The quadrupole focusing term is $K_Q^2 = |qB_o/r_Q|/(\gamma_c\beta_c mc)$, where B_o is the magnetic field and r_Q is the characteristic gradient scale length and $B_o/r_Q \sim 5$kG/cm. The RF focusing/defocusing term is $K_{RF,\perp}^2 = \pi q E_{RF}/(mc^2\gamma_c^3\beta_c^3\lambda_{RF})\cos\Psi_c$. The energy associated with the bunch centroid is given by

$$\frac{\partial\gamma_c}{\partial z} = \frac{qE_{RF}}{mc^2}\beta_c\sin(\Psi_c), \tag{12}$$

where $\gamma_c = (1 - \beta_c^2)^{-1/2}$.

IV. FEL Amplifier Wall-Plug Efficiency

In this section we calculate the FEL wall-plug efficiency for a tapered amplifier configuration. We numerically solve Eqs. (11) and (12) using electron beam parameters appropriate to a high-power FEL. Figure 4 shows a tapered FEL amplifier configuration in which the electron beam from an RF gun is accelerated in the linac, enters a tapered FEL wiggler, generates FEL radiation, and emerges as a spent beam consisting of trapped and un-trapped particles. The spent electron bunch is shown schematically in Fig. 5. Figure 5(a) shows the initial electron beam distribution exiting the FEL wiggler. Injecting these two populations at the same phase of the RF wave causes them to be de-accelerated to the final configuration shown in Fig. 5(b) in which the trapped particles have a minimum energy of $E_{\min}$ and the un-trapped particles have a minimum energy of $\sim E_{\min} + \eta_{FEL} E_b$. The un-trapped particles can be de-accelerated to $E_{\min}$ by injecting them at a different phase relative to the trapped particles, i.e., one for which the de-accelerating field is larger, as shown in Fig. 5(c). This increases the recovered energy by an additional amount $\sim \eta_{FEL} E_b$, which increases the overall wall-plug efficiency.

In the example that follows, the RF linac field is assumed to have a wavelength of 40 cm and an accelerating gradient of 15 MeV/m. The accelerating/de-accelerating cavity is 5.5 m long. An external quadrupole focusing field with normalized amplitude $qB_o/(amc^2) = 0.02\,\mathrm{cm}^{-2}$ is assumed.

The initial electron bunch before acceleration in the linac is assumed to have the parameters listed in Table 1, e.g., energy of 5 MeV and a bunch charge of 1 nC. Injecting the bunch at an initial phase of $\Psi_{c0} = 1.9$, it is accelerated to ~ 83 MeV at the end of linac as shown in Fig. 6(a). The energy spread decreases from 0.12% to 0.008% during acceleration (Fig. 6(b)) and the bunch length remains relatively contstant (Fig. 7(a)). The bunch radius undergoes oscillation due to the RF and external focusing fields (Fig 7(b).

Before entering the wiggler, the beam is focused to a spot size of 0.2 mm and compressed to ~1 psec to increase the peak current for the FEL interaction in a tapered wiggler. At the wiggler exit, the bunch length is ~ 1 psec and the trapped and un-trapped particles are assumed to have a longitudinal emittance of $\varepsilon_{n,z}^2 \sim 2.5\,\mathrm{MeV} - \mathrm{psec} \sim 2500$

keV-psec. This corresponds to a fractional energy spread of ~ 3%. In a properly tapered wiggler, ~ 80% of the particles can be trapped.

Before re-entering the linac to be de-accelerated, it is assumed that the bunch is lengthened to 5 psec to reduce the energy spread. The trapped particles are injected at a phase $\Psi_0 = 4.18$ and the un-trapped particles are injected at $\Psi_0 = 4.73$. This causes both populations to be de-accelerated to a final energy < 2 MeV at the end of the linac, as shown in Fig. 6(a). Figure 6(b) shows that the fractional energy spread of the trapped particles increases to > 30% near the end of the linac before decreasing to a value of ~ 7% at the exit. The un-trapped particles have a final energy spread of ~ 18%. The bunch length of the trapped and un-trapped particles remains relatively constant until the end of the linac where the trapped particles cause the bunch length to increase to ~ 2.5% of the RF wavelength [Fig. 7(a)]. The final bunch radius of the trapped particles is ~0.1 cm.

Figure 8 shows the wall-plug efficiency for oscillator (green curve), un-tapered amplifier (blue curve), and tapered amplifier (red curves) configurations versus minimum beam energy. For the tapered amplifier, the solid red curve denotes the case where trapped and un-trapped particles are injected at the same phase, $\Psi_0 = 4.18$. The dashed curve denotes the case for which trapped and un-trapped particles are injected at different phases, i.e., $\Psi_0 = 4.18$ for trapped particles and $\Psi_0 = 4.73$ for un-trapped particles. The parameters for Fig. 8 are $E_b = 80$ MeV, $I_b = 1$ A, $\eta_{RF} = 0.6$, $P_{\text{cryo}} = 1$ MW, $\eta = 0.6$, $\varepsilon = 0.3$, $\eta_{\text{inj}} = 0.6$, and $\beta = 1$.

V. Conclusions

We have calculated the wall-plug efficiency for an FEL oscillator, amplifier, and tapered amplifier configuration employing an energy recovery linac. The wall-plug efficiency depends on various FEL-ERL parameters and can be improved, for example, by reducing the minimum energy entering the beam dump, E_{min}. By reducing E_{min} from 4 MeV to 2 MeV and keeping all other parameters the same the wall-plug efficiency for the oscillator increases from 10% to 12%; for the uniform wiggler amplifier the efficiency increases from 10% to 14%; and for the tapered wiggler amplifier the efficiency increases from 22% to 24%. For typical MW class FEL parameters, we find

that the wall-plug efficiency for the oscillator is in the range $\eta_{WP} \approx 10-15\%$ For the uniform wiggler amplifier $\eta_{WP} \approx 10-15\%$, and for the tapered wiggler amplifier $\eta_{WP} \approx 20-25\%$

Acknowledgments: The work was sponsored by the Office of Naval Research and the Joint Technology Office.

Appendix

The longitudinal and transverse dynamics of a relativistic charge bunch are described by a set of coupled envelope equations for the root mean square (rms) bunch length and radius. The bunch length and radius dynamics are determined by the effects of the RF linac field, space charge fields, inductive (self magnetic) fields, external focusing fields as well as the axial and transverse energy spreads (emittances).

I. Fields

a) Space Charge Fields [6-8]

The potential associated with a stationary (beam frame) elliptical charge bunch of uniform density, with radial and axial semi-axis of (a, z_m) in the beam frame, centered at $z = 0$ is

$$\Phi(r,z) = -2\pi\rho_o\left(\frac{(1-M(\xi))}{2}r^2 + M(\xi)z^2\right), \qquad \text{(A1)}$$

where the charge density is $\rho_o = (3/4\pi)qN/(a^2 z_m)$, qN is the charge in the bunch. The uniform charge ellipse is defined by $r^2/a^2 + z^2/z_m^2 \le 1$. The electro-static space charge field in the beam frame is $\mathbf{E}_{sc} = -\nabla\Phi$. In the beam frame the function $M(\xi)$ depends on the aspect ratio and geometry. In the absence of walls $M(\xi)$ is a function of only the aspect ratio, $\xi = (1 - a^2/z_m^2)^{1/2}$.

In the laboratory frame the space charge fields are modified by both relativistic and inductive effects. In the laboratory frame where the bunch is moving with constant axial velocity v, the scalar potential is, in the Lorentz gauge, given by $\left(\nabla_\perp^2 + (1/\gamma^2)\partial^2/\partial\eta^2\right)\Phi(r,\eta) = -4\pi\rho(r,\eta)$ where $\eta = z - vt$, $\gamma = (1 - v^2/c^2)^{-1/2}$ and ρ is the charge density. In the laboratory frame there exists an axial vector potential

given by $A = (v/c)\Phi$ which results in an inductive axial electric field. The rms bunch radius and length, in the laboratory frame, are given by $R_b = \langle r^2 \rangle^{1/2} = a/\sqrt{5}$ and $L_b = \langle z^2 \rangle^{1/2} = z_m/(\sqrt{5}\gamma)$, respectively. The scalar potential in the laboratory frame is found from the expression for the potential in the beam frame, Eq. (A1), by replacing the variable z with $\gamma\eta$ and the density with $\rho_o = (3/4\pi)(1/10\sqrt{5})qN/(R_b^2 L_b)$. The potential in the laboratory frame becomes,

$$\Phi(r,\eta) = -\frac{3}{10\sqrt{5}}\frac{qN}{R_b^2 L_b}\left(\frac{(1-M(\xi))}{2}r^2 + M(\xi)\gamma^2\eta^2\right), \tag{A2}$$

where

$$M(\xi) = \frac{1-\xi^2}{2\xi^3}\left(\ln\left(\frac{1+\xi}{1-\xi}\right) - 2\xi\right), \tag{A3}$$

and $\xi = (1-(R_b/\gamma L_b)^2)^{1/2}$. The expression for $M(\xi)$ is valid for the full range of the ratio $R_b/(\gamma L_b)$ and is shown in Fig. 3. The axial and radial self electric fields of the bunch, centered at $r = 0$, $z = z_c = v_c t$, in the laboratory frame

$$E_{sc,z}(\eta) = -\frac{1}{\gamma^2}\frac{\partial\Phi}{\partial\eta} = \frac{3}{5\sqrt{5}}\frac{qN}{R_b^2 L_b}M(\xi)(z - z_c(t)), \tag{A4a}$$

$$E_{sc,r}(r) = -\frac{\partial\Phi}{\partial r} = \frac{3}{10\sqrt{5}}\frac{qN}{R_b^2 L_b}(1-M(\xi))r, \tag{A4b}$$

b) ERL Fields

The ERL electric and magnetic fields near the axis are given by

$$E_{RF,z}(z,t) = E_{RF}\sin\left(\int_0^z k_{RF}(z')dz' + \omega_{RF}t\right), \tag{A5a}$$

$$E_{RF,r}(z,t) = -E_{RF}(k_{RF}r/2)\cos\left(\int_0^z k_{RF}(z')dz' + \omega_{RF}t\right), \tag{A5b}$$

$$B_{RF,\theta}(r,z,t) = -E_{RF}(\omega_{RF}r/2c)\cos\left(\int_0^z k_{RF}(z')dz' + \omega_{RF}t\right), \tag{A5c}$$

E_{RF} is the field amplitude, ω_{RF} is the RF frequency and $k_{RF} = 2\pi/\lambda_{RF}$ is the local wavenumber of the RF field.

II. Bunch Dynamics

a) Longitudinal Bunch Dynamics

The relativistic longitudinal electron motion is given by

$$\frac{\partial^2 z}{\partial t^2} = \frac{q}{\gamma^3 m}\left(E_{RF}\sin\left(\int^{z} dz' k_{RF}(z') - \omega_{RF} t \right) + E_{sc,z}(z,t) \right), \tag{A6}$$

where $z(t)$ is the axial electron position and $\gamma(t) = \left(1 - (\partial z/\partial t)^2/c^2\right)^{-1/2}$. The axial electron position can be written as $z(t) = z_c(t) + \delta z(t)$, where δz is the axial position relative to the centroid. The equation of motion of the centroid of the bunch is given by

$$\frac{\partial^2 z_c(t)}{\partial t^2} = \frac{\Omega_{RF}^2}{k_{RF}}\sin\left(\Psi_c(t)\right), \tag{A7}$$

while $\delta z(t)$ is given by

$$\frac{\partial^2 \delta z}{\partial t^2} = \frac{\Omega_{RF}^2}{k_{RF}}\left(\sin\left(\Psi_c + \int_{z_c}^{z_c+\delta z} dz' k_{RF}(z') \right) - \sin(\Psi_c) \right) + \Omega_{sc,z}^2 \delta z - \frac{3}{\gamma_c}\frac{\partial \gamma_c}{\partial t}\frac{\partial \delta z}{\partial t}, \tag{A8}$$

where $\Psi_c(t) = \int_0^{z_c} dz' k_{RF}(z') - \omega_{RF} t + \Psi_c(0)$, $\Omega_{sc,z}^2 = 3/(5\sqrt{5})(q^2 N/m) M/(\gamma_c^3 R_b^2 L_b)$, $\Omega_{RF}^2 = q E_{RF} k_{RF}/(\gamma_c^3 m)$, $k_{RF} = k_{RF}(z_c(t))$, $\gamma_c = (1-\beta_c^2)^{-1/2}$ and $\beta_c = c^{-1}\partial z_c/\partial t$. The energy associated with the bunch centroid is given by

$$\frac{\partial \gamma_c}{\partial t} = \frac{\Omega_{RF}^2}{c k_{RF}}\gamma_c^3 \beta_c \sin(\Psi_c) = \frac{q E_{RF}}{mc}\beta_c \sin(\Psi_c). \tag{A9}$$

For k_{RF} constant and $|k_{RF}\,\delta z| << 1$ we can write

$$\frac{\partial^2 \delta z}{\partial t^2} - \Omega_z^2 \delta z + \frac{3}{\gamma_c}\frac{\partial \gamma_c}{\partial t}\frac{\partial \delta z}{\partial t} = 0, \tag{A10}$$

where $\Omega_z^2 = \Omega_{RF}^2 \cos\Psi_c + \Omega_{sc,z}^2$, $\Psi_c = k_{RF} z_c - \omega_{RF} t$, $\ddot{z}_c = q E_{RF}/(\gamma_c^3 m)\sin(\Psi_c)$ and the overdot indicates $\partial/\partial t$.

The longitudinal electron motion about the centroid is given by Eq. (A10), which upon multiplying by δz and $\delta \dot{z}$ and combining the resulting averaged equations leads to

$$\left(3\frac{\dot{\gamma}_c}{\gamma_c} + \frac{1}{2}\frac{\partial}{\partial t}\right)\left(L_b \ddot{L}_b + (\dot{L}_b)^2 - \Omega_z^2 L_b^2 + 3\gamma_c^{-1}\dot{\gamma}_c L_b \dot{L}_b\right) - \Omega_z^2 L_b \dot{L}_b = 0, \quad \text{(A11)}$$

where $L_b = \langle \delta z^2 \rangle^{1/2}$ is the rms bunch length. It can be shown that the above equation can be written as a total derivative,

$$\frac{\partial}{\partial t}\left(\gamma_c^6 \left(L_b^3 \dot{L}_b - \Omega_z^2 L_b^4 + 3\gamma_c^{-1}\dot{\gamma}_c L_b^3 \dot{L}_b\right)\right) = 0, \quad \text{(A12)}$$

and $\gamma_c^6 L_b^2\left(L_b \dot{L}_b - \Omega_z^2 L_b^2 + 3\gamma_c^{-1}\dot{\gamma}_c L_b \dot{L}_b\right) = c^2 \varepsilon_{n,z}^2$, where $\varepsilon_{n,z}$ is the constant normalized longitudinal emittance. Since $L_b \ddot{L}_b - \Omega_z^2 L_b^2 + 3\gamma_c^{-1}\dot{\gamma}_c L_b \dot{L}_b = \langle \delta v^2 \rangle - \dot{L}_b^2$, we can write the emittance term as $c^2 \varepsilon_{n\,z}^2 = \gamma_c^6 L_b^2\left(\langle \delta v^2 \rangle - (\dot{L}_b)^2\right)$ where $\delta v = \delta \dot{z}$. Assuming self-similar behavior, $\delta v = \delta z \dot{L}_b / L_b + v_{th}$, the normalized longitudinal emittance becomes

$$\varepsilon_{n\,z}^2 = \frac{\gamma_c^6 L_b^2}{c^2}\left(\langle \delta v^2 \rangle - (\dot{L}_b)^2\right) = \gamma_c^6 L_b^2 \frac{v_{th}^2}{c^2} = \frac{c^2 L_b^2}{v_c^2}\gamma_{th}^2. \quad \text{(A13)}$$

The longitudinal envelope equation for the bunch is

$$\frac{\partial^2 L_b}{\partial t^2} - \Omega_z^2 L_b + \frac{3}{\gamma_c}\frac{\partial \gamma_c}{\partial t}\frac{\partial L_b}{\partial t} - \frac{c^2 \varepsilon_{n\,z}^2}{\gamma_c^6 L_b^3} = 0. \quad \text{(A14)}$$

The normalized longitudinal emittance $\varepsilon_{n,z} = L_b \gamma_{th} / \beta_c$ is a Lorentz invariant which is also commonly written as $\varepsilon_{n,z} = \varepsilon_{n\,z}^* / mc$ where $(1/mc) = 5.87\times10^4$ [cm/(eV−sec)], $\varepsilon_{n,z}^* = \Delta E_b \Delta \tau_b$ [eV−sec] and $\Delta \tau_b = L_b / v_c$ is the bunch duration [9].

b) Transverse Bunch Dynamics

Using a similar approach an envelop equation for the rms bunch radius can be obtained. The radial electron motion about the center of the bunch is given by $\delta \ddot{r} - \Omega_\perp^2 \delta r + \gamma_c^{-1}\dot{\gamma}_c \delta \dot{r} = 0$, where $\Omega_\perp^2 = \Omega_{sc,\perp}^2 - \Omega_o^2$, $\Omega_{sc\,\perp}^2 = 3/(10\sqrt{5})q^2 N/(\gamma_c^3 m)(1-M)/(R_b^2 L_b)$ is due to the transverse self fields and Ω_o^2 represents external transverse defocusing or focusing due to the RF and quadrupole fields. The transverse envelope equation is

$$\frac{\partial^2 R_b}{\partial t^2} + \frac{1}{\gamma_c}\frac{\partial \gamma_c}{\partial t}\frac{\partial R_b}{\partial t} - \Omega_\perp^2 R_b - \frac{c^2 \varepsilon_{n\perp}^2}{\gamma_c^2 R_b^3} = 0, \quad \text{(A15)}$$

where $\varepsilon_{n\perp}$ is the rms normalized transverse emittance.

c) Change of Variables

It is useful to employ the axial coordinate z as the independent variable instead of the time t. Performing this transformation the equations become

$$\frac{\partial^2 L_b}{\partial z^2} + \left(3 + \frac{1}{\beta_c^2 \gamma_c^2}\right)\frac{1}{\gamma_c}\frac{\partial \gamma_c}{\partial z}\frac{\partial L_b}{\partial z} - K_z^2 L_b - \frac{\varepsilon_{n,z}^2}{\beta_c^2 \gamma_c^6 L_b^3} = 0, \tag{A16a}$$

$$\frac{\partial^2 R_b}{\partial z^2} + \frac{1}{\beta_c^2 \gamma_c}\frac{\partial \gamma_c}{\partial z}\frac{\partial R_b}{\partial z} - K_\perp^2 R_b - \frac{\varepsilon_{n,\perp}^2}{\beta_c^2 \gamma_c^2 R_b^3} = 0, \tag{A16b}$$

$$\frac{\partial \gamma_c}{\partial z} = \frac{q E_{RF}}{mc^2}\beta_c \sin(\Psi_c), \tag{A16c}$$

where $K_z^2 = K_{RF}^2 \cos\Psi_c + K_{sc,z}^2$, $K_\perp^2 = K_{sc,\perp}^2 - K_{RF,\perp}^2 - K_Q^2$,

$K_{sc,z}^2 = 3/(5\sqrt{5})(q^2 N/m)M/(c^2 \beta_c^2 \gamma_c^3 R_b^2 L_b)$,

$\Psi_c = \int_0^z (k_{RF}(z') - \omega_{RF}/(c\beta_c(z')))dz' + \Psi_c(0)$,

$K_{sc,\perp}^2 = 3/(10\sqrt{5})q^2 N/(mc^2)(1 - M(\xi))/(\beta_c^2 \gamma_c^3 R_b^2 L_b)$, $K_{RF}^2 = q E_{RF} k_{RF}/(mc^2 \beta_c^2 \gamma_c^3)$,

$K_{RF,\perp}^2 = \pi q E_{RF}/(mc^2 \gamma_c^3 \beta_c^3 \lambda_{RF})\cos\Psi_c$ is due to RF focusing/defocusing, and

$K_Q^2 = |q B_o / r_Q|/(\gamma_c \beta_c mc)$ is due to quadrupole focusing, B_o is the magnetic field and r_Q is the characteristic gradient scale length.

References

[1] "High Average Power Optical FEL Amplifiers," I. Ben-Zvi, D. Kayran and V. Litvinenko, (2005) International FEL Conference, Stanford, CA, p. 232

[2] "Short Rayleigh Length Free Electron Lasers,'' W. B. Colson, J. Blau, R. L. Armstead, P. P. Crooker, R. Vigil, T Voughs, and B. W. Williams, Phys. Rev. ST Accel. Beams **9**, 030703 (2006)

[3] "The JLab High Power ERL Light Source,'' Proceedings ERL '05 Workshop, Newport News, VA, March 20-23, (2005)

[4] "Design of a Compact, Optically Guided, Pinched, Megawatt Class Free-Electron Laser," P. Sprangle, B. Hafizi and J.R. Peñano, IEEE J. Quantum Electron. **40**, 1739 (2004)

[5] "Nonlinear Theory of Free-Electron Lasers and Efficiency Enhancement," P. Sprangle, C.M. Tang and W.M Manheimer, Phys. Rev. A **21**, 302 (1980)

[6] M. Reiser, "Theory and Design of Charged Particle Beams," Wiley, New York, 1994.

[7] T. Wangler, "RF Linear Accelerators," Wiley, New York, 1998.

[8] P.M. Lapostolle, "Effets de la Charge d'Espace dans un Accélérateur Linéaire a Proton," CERN Report AR/Int. SG/65-15, 1965.

[9] For the FEL beam at the Jefferson-Laboratory, $\varepsilon^*_{n,z} = \Delta E_b \, \Delta \tau_b [\mathrm{eV-sec}] \approx 100\,\mathrm{keV-psec}$ and $\varepsilon_{n\,z} \approx 6\times10^{-3}\,\mathrm{cm}$.

Bunch parameters	**Initial bunch**	**Trapped particles after wiggler**	**Un-trapped particles after wiggler**
Energy (MeV)	5	70	83
Longitudinal emittance [keV-psec]	100	2500	2500
Transverse emittance [mm-mrad]	5	5	5
Bunch length [psec]	15	5	5
Energy spread [%]	0.12	0.7	0.6
Radius [mm]	1	0.2	0.2
Bunch charge [nC]	1	0.8	0.2
Injection phase [rad]	1.9	4.18	4.73

Table 1: Electron bunch input parameters used in the numerical examples of Figures 6 and 7.

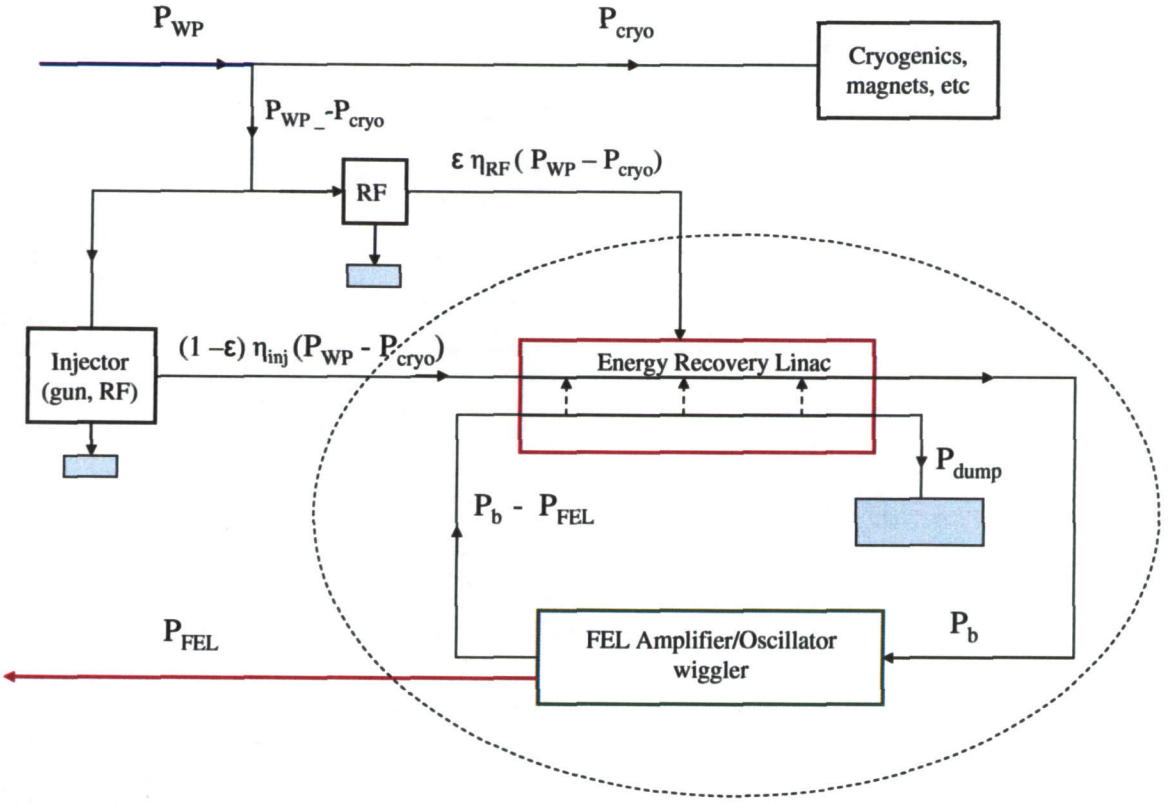

Figure 1: Power flow diagram of an FEL employing an ERL which is used to derive the wall-plug efficiency.

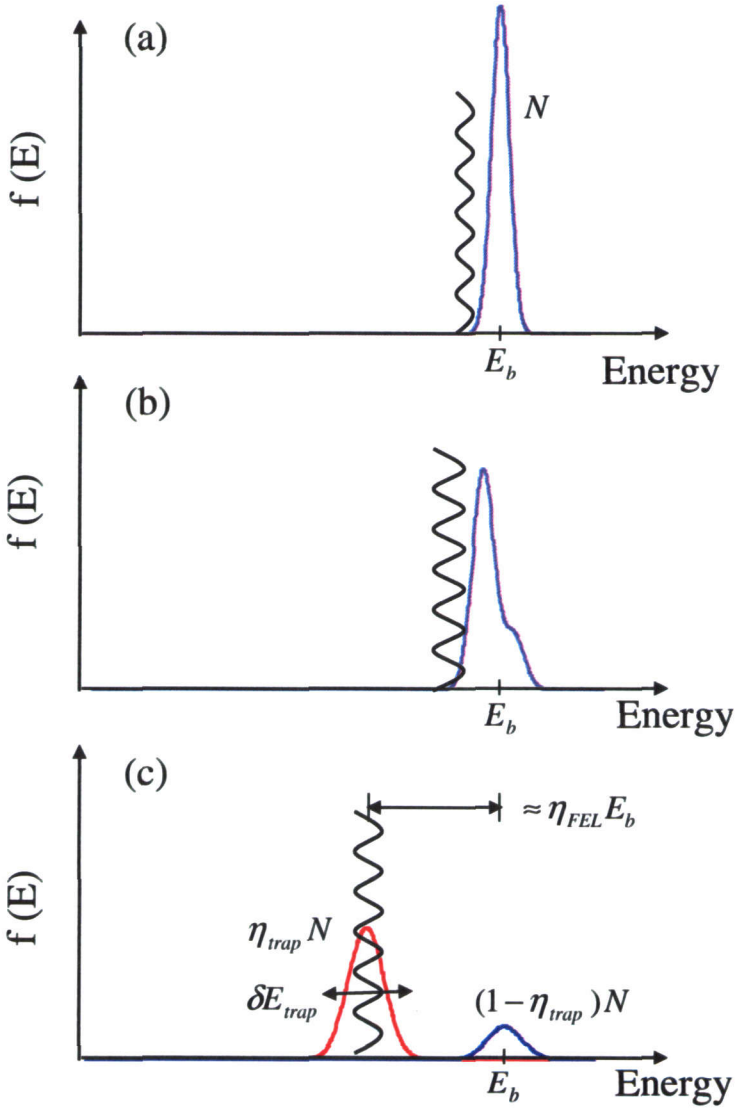

Figure 2: Illustration of the electron energy distribution in a tapered FEL amplifier. (a) shows the electron distribution function at the wiggler entrance ($z = 0$), a beam of N electrons with energy E_b. (b) shows the electron distribution at the tapered wiggler exit ($z = L_w$). A fraction of electrons η_{trap} are trapped and de-accelerated to an average energy $E_b - \Delta E_b$. The trapped particles have an induced energy spread δE_{trap}. (c) shows the electron distribution at the beam dump. Both trapped and un-trapped electrons are de-accelerated by an amount $E_b - \Delta E_b - (\delta E_{trap}/2) - E_{\min}$. The total energy entering the beam dump in (c) is given by Eq. (5)

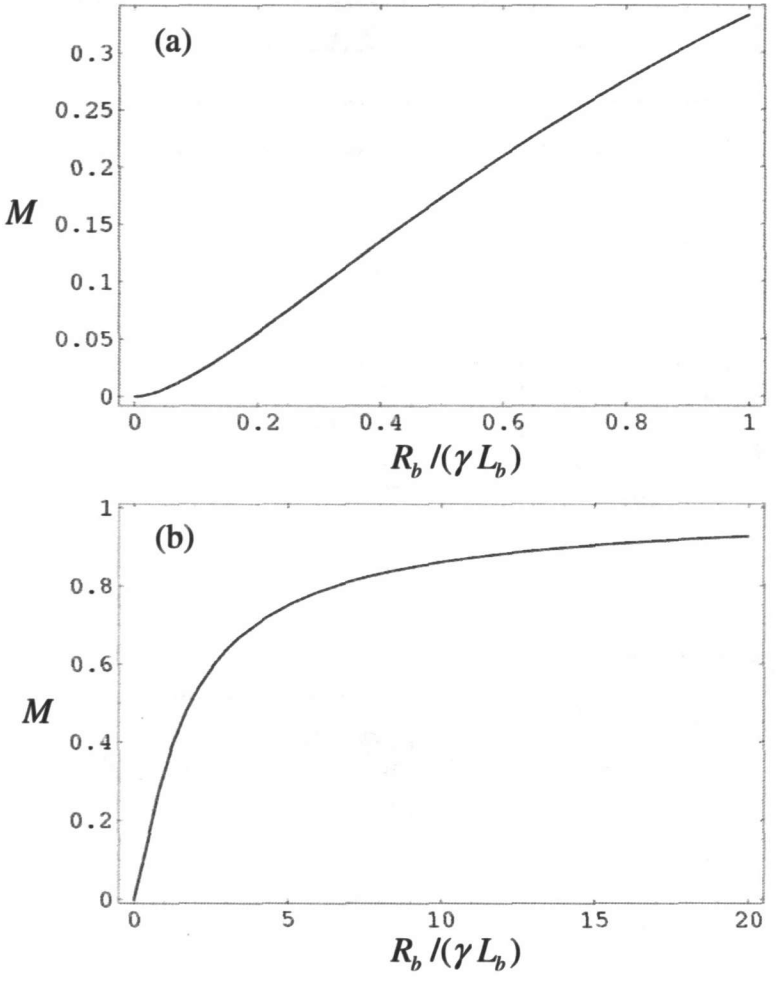

Figure 3: Plot of the space charge function M versus $R_b/(\gamma L_b)$, Eq. (9). The self-fields of an ellipsoidal charge with length L_b and radius R_b are expressible in terms of M as given in Eq. (8). In (a) the function M is plotted for $0 \le R_b/(\gamma L_b) \le 1$, while in (b), the range of $R_b/(\gamma L_b)$ is extended to 20.

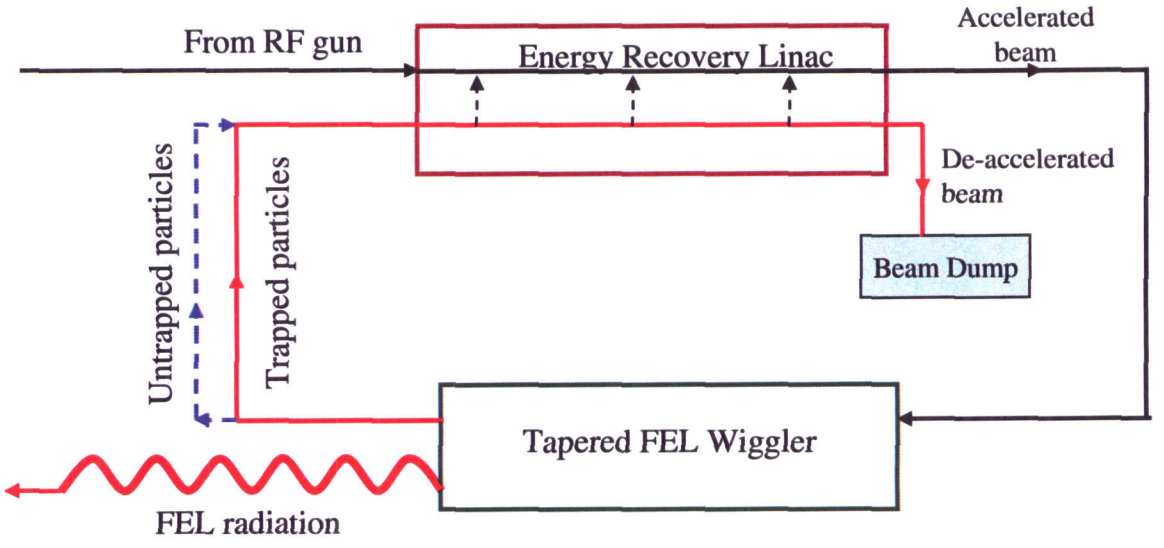

Figure 4: Schematic diagram showing the electron beam from an RF gun being accelerated in the linac, entering a tapered FEL wiggler, generating FEL radiation, and emerging as a spent beam consisting of trapped and un-trapped particles. The trapped and un-trapped particles are then injected into the linac at different phases and de-accelerated to recover most of their energy before being sent to a beam dump.

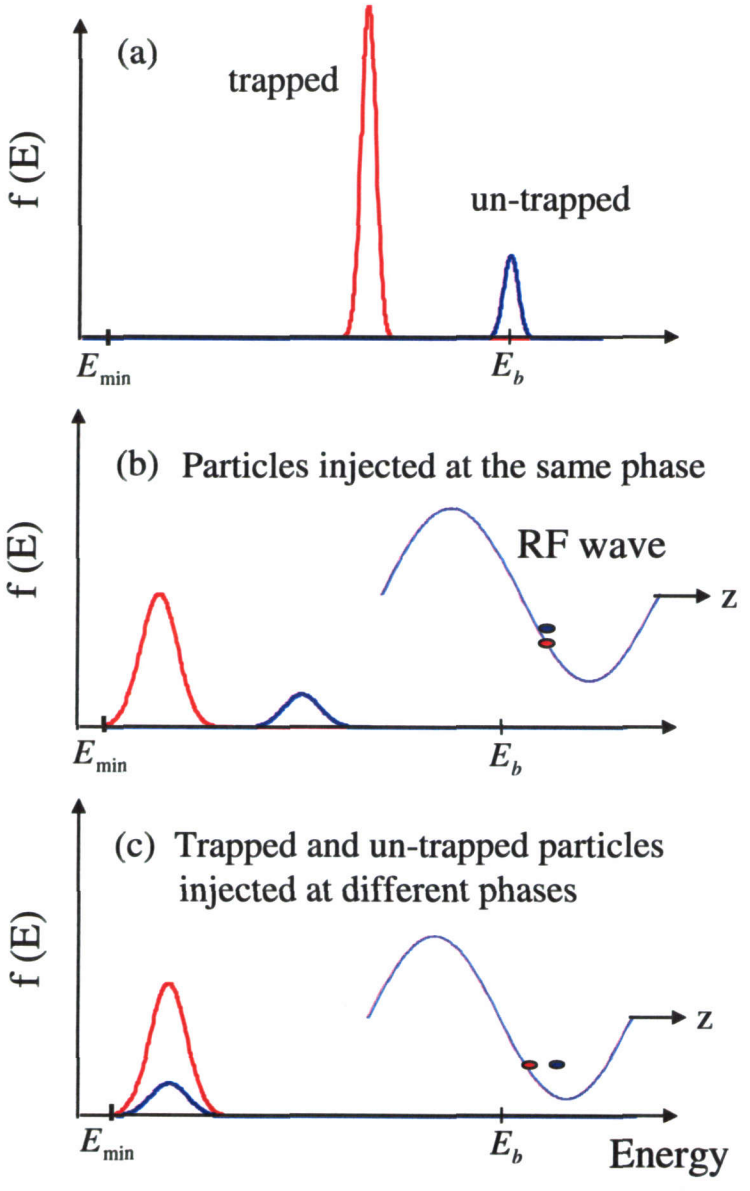

Figure 5: Schematic diagram showing the trapped (red) and untrapped (blue) electron energy distributions (a) at the end of the tapered wiggler, and after energy recovery when (b) the particles are injected at the same RF phase, and (c) the trapped and untrapped particles are injected at different phases in order to de-accelerate them to the same minimum energy and enhance wall-plug efficiency.

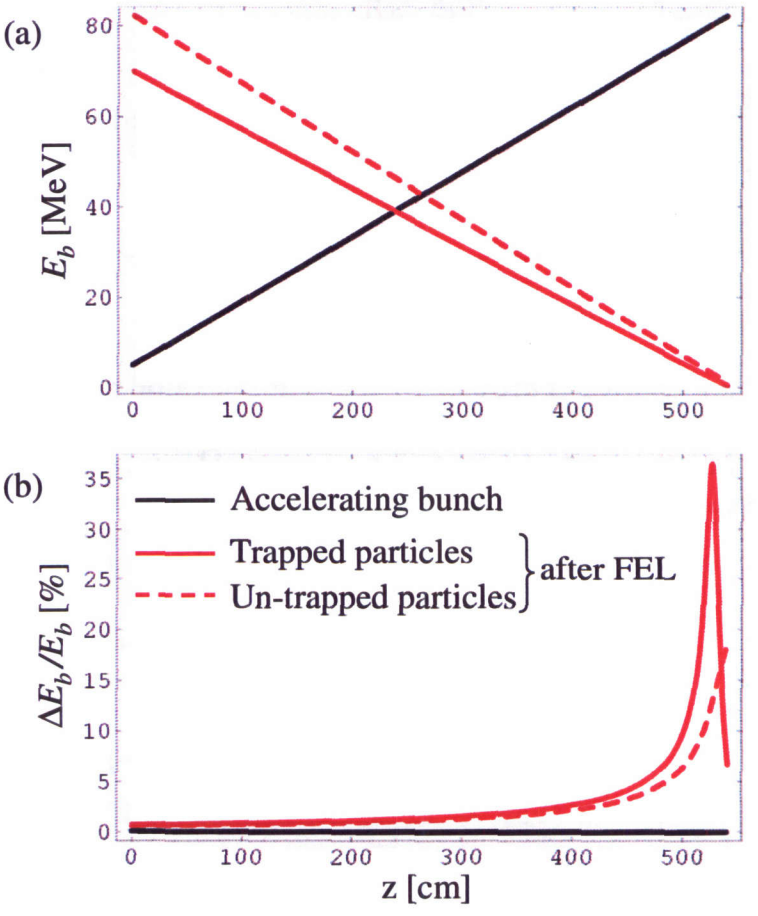

Figure 6: Beam energy (a) and energy spread (b) versus longitudinal position, z, within the linac. Curves denote the electron bunch before the FEL interaction (black curves), and the trapped (solid red curves) and untrapped (dashed red curves) particles after the FEL interaction in a tapered amplifier. Parameters are listed in Table 1.

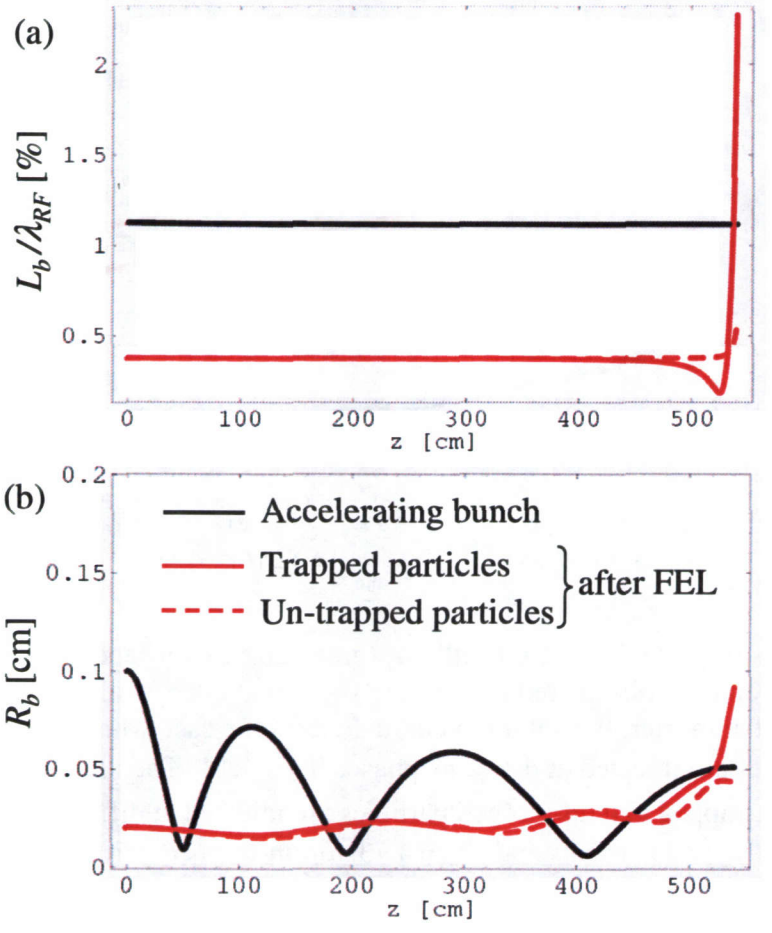

Figure 7: Bunch length normalized to RF wavelength (a) and bunch radius (b) versus longitudinal position, z, within the linac. Curves denote the electron bunch before the FEL interaction (black curves), and the trapped (solid red curves) and untrapped (dashed red curves) particles after the FEL interaction in a tapered amplifier. Parameters are listed in Table 1.

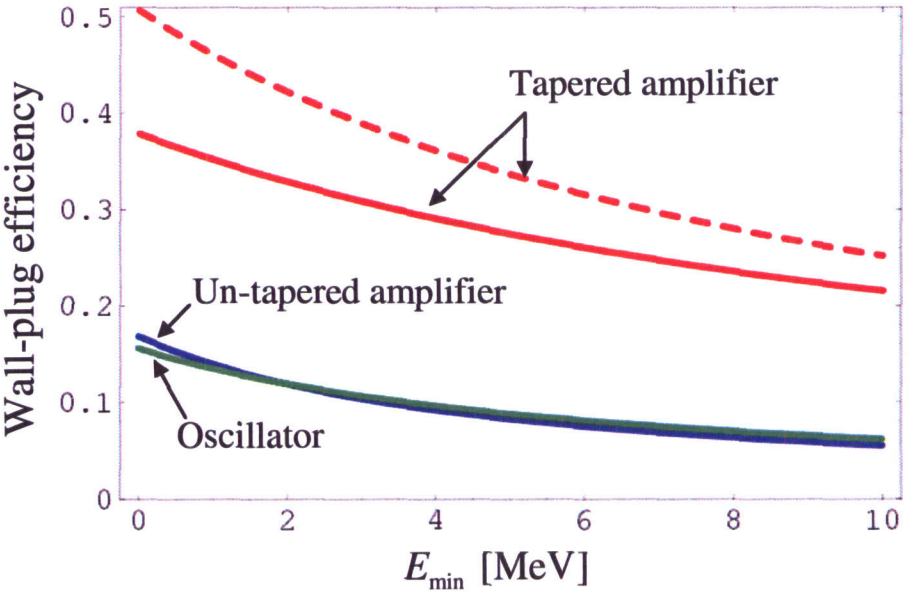

Figure 8: Wall-plug efficiency for oscillator (green curve), un-tapered amplifier (blue curve), and tapered amplifier (red curves) configurations versus minimum beam energy. For the tapered amplifier, the solid red curve denotes the case where trapped and un-trapped particles are injected at the same phase, $\Psi_0 = 4.18$. The dashed curve denotes the case for which trapped and un-trapped particles are injected at different phases, i.e., $\Psi_0 = 4.18$ for trapped particles and $\Psi_0 = 4.73$ for un-trapped particles. ERL parameters are $E_b = 80$ MeV, $I_b = 1$ A, $\eta_{RF} = 0.6$, $P_{cryo} = 1$ MW, $\eta = 0.6$, $\varepsilon = 0.3$, $\eta_{inj} = 0.6$, and $\beta = 1$.